9th Asia-Pacific Conference on Wind Engineering
Auckland, New Zealand
3-7 December 2017

Modelling of distributed Aerodynamic and Aeroelastic Pressures on Bridge Deck Based on Proper Orthogonal Decomposition

Z.X. Tan[1,2,3], Y.L. Xu[1], L.D. Zhu[2,3] and Q. Zhu[2,3]

[1] Department of Civil and Environmental Engineering
The Hong Kong Polytechnic University, Hong Kong, China

[2] State Key Laboratory of Disaster Reduction in Civil Engineering
Tongji University, Shanghai, China

[3] Department of Bridge Engineering, College of Civil Engineering
Tongji University, Shanghai, China

Abstract

An accurate model of distributed aerodynamic and aeroelastic pressures on bridge decks is crucial to the stress-level analysis of long-span bridges. This study firstly proposes a framework for modelling distributed aerodynamic and aeroelastic pressures on a bridge deck using the proper orthogonal decomposition (POD), in which the indicial functions are introduced to feature the unsteady components associated with different structural motion and wind turbulence. The POD pressure modes, pressure modal derivatives, distributed aerodynamic and aeroelastic pressures, integrated aerodynamic and aeroelastic force, and force derivatives of a typical twin-box bridge deck are then identified and discussed as a case study.

1. Introduction

The stress-level analysis is important for assessing the performance and safety of long-span bridges, which requires an appropriate model of wind-induced fluctuating pressures on bridge decks. However, it is not easy to describe the distributed aerodynamic and aeroelastic pressures on the surfaces of a bridge deck. Therefore, the POD method has been introduced in the analysis of random pressure fields around bridge decks [1,2]. On the other hand, the modelling schemes of wind-induced loads, including both aerodynamic and aeroelastic effects, have been summarized by Wu [3], in which the semi-empirical linear model is the most widely used approach. The buffeting and self-excited loads are usually taken into account by using separately identified aerodynamic admittances and flutter derivatives, and the two components are regarded as simply additive without interaction. The unsteady effect is taken into account by introducing the indicial function [3,5], which is also known as a fitting scheme to approximate the corresponding derivatives. Analogously, the semi-empirical linear model can be applied to the POD pressure model to describe the distributed aerodynamic and aeroelastic pressures on a bridge deck, which is the focus of this paper.

2. POD Mode of Aerodynamic and Aeroelastic Pressures

2.1. POD Pressure Modes

The wind-induced fluctuating pressure with aerodynamic and aeroelastic components at a point can be expressed as

$$P_i(t)=\frac{1}{2}\rho\bar{U}^2\left\{2C_{p_i}\frac{u(t)}{\bar{U}}+C'_{p_i}\left[\beta(t)+\frac{w(t)-\dot{h}(t)-b\dot{\beta}(t)}{\bar{U}}\right]\right\} \tag{1}$$

where ρ is the density of air; $\bar{U}$ is the mean speed of incoming wind; u and w are the longitudinal and vertical turbulent components; h and β are the vertical and torsion motions, respectively; C_{p_i} and C'_{p_i} are the pressure coefficient and its derivative defined in the structural coordinate system (see Figure 1); and b is a characteristic length of the section.

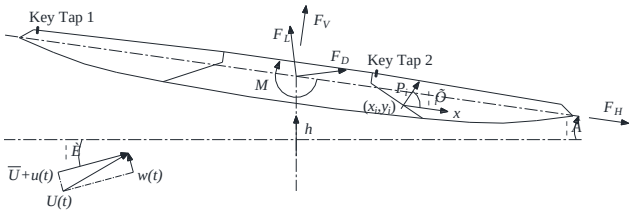

Figure 1 Deck section and coordinate system

By using POD, the fluctuating pressures on a bridge deck can be represented as the superposition of the products of principal coordinates and uncorrelated space functions (also known as POD modes). The distributed pressures can thus be expressed as

$$\boldsymbol{P}(t)=\boldsymbol{\Phi}\mathbf{A}(t)=\sum_{j=1}^{N}\alpha_j(t)\boldsymbol{\phi}_j \tag{2}$$

where $\boldsymbol{P}(t)=\{P_1(t),\cdots,P_N(t)\}^T$ is the matrix of distributed pressures; $\boldsymbol{\Phi}=\{\boldsymbol{\phi}_1,\cdots,\boldsymbol{\phi}_N\}$ and $\mathbf{A}(t)=\{\alpha_1(t),\cdots,\alpha_N(t)\}^T$ are the space function matrix and the principal coordinate matrix of the POD pressure modes, respectively.

By introducing the pressure modal coefficient and its derivative, $C_{\alpha_j}=\sum C_{p_i}\phi_{ij}$ and $C'_{\alpha_j}=\sum C'_{p_i}\phi_{ij}$, the principal coordinate of each pressure mode can be calculated by

$$\alpha_j(t)=\frac{1}{2}\rho\bar{U}^2\left\{2C_{\alpha_j}\frac{u(t)}{\bar{U}}+C'_{\alpha_j}\left[\beta(t)+\frac{w(t)-\dot{h}(t)-b\dot{\beta}(t)}{\bar{U}}\right]\right\} \tag{3}$$

2.2. Pressure Modal Derivatives

By adopting the Scanlan's formulation for aerodynamic and aeroelastic forces in the pure time domain [4], the principal coordinate expressed by Eq.(3) can be rewritten in a time-dimensionless form in terms of indicial functions.

$$\begin{aligned}\alpha_j(s)=\frac{1}{2}\rho\bar{U}^2\int_0^s\Bigg[&2C_{\alpha_j}\varphi_{\alpha_j u}(s-\sigma)\frac{u'(\sigma)}{\bar{U}}+C'_{\alpha_j}\varphi_{\alpha_j w}(s-\sigma)\frac{w'(\sigma)}{\bar{U}}\\&-C'_{\alpha_j}\varphi_{\alpha_j h}(s-\sigma)\frac{h''(\sigma)}{B}+C'_{\alpha_j}\varphi_{\alpha_j\beta}(s-\sigma)\beta'(\sigma)\Bigg]d\sigma\end{aligned} \tag{4}$$

where $\varphi_{\alpha_j x}$ (x= u, w, h, β) is the indicial function representing the transient evolutionary characteristic of the principal coordinate of the j^{th} pressure mode. It has the following general form.

$$\varphi(s)=1-a_1e^{-d_1 s}-a_2e^{-d_2 s} \tag{5}$$

By using the integration by parts and the Fourier transform, the principal coordinate can be expressed as

$$\hat{\alpha}_j(K)=\frac{1}{2}\rho\bar{U}^2\left\{2C_{\alpha_j}\left[\varphi_{\alpha_j u}(0)+\hat{\varphi}'_{\alpha_j u}(K)\right]\frac{\hat{u}(K)}{\bar{U}}+C'_{\alpha_j}\left[\varphi_{\alpha_j w}(0)+\hat{\varphi}'_{\alpha_j w}(K)\right]\frac{\hat{w}(K)}{\bar{U}}\right.$$
$$\left.-C'_{\alpha_j}\left[\varphi_{\alpha_j h}(0)+\hat{\varphi}'_{\alpha_j h}(K)\right]iK\frac{\hat{h}(K)}{B}+C'_{\alpha_j}\left[\varphi_{\alpha_j \beta}(0)+\hat{\varphi}'_{\alpha_j \beta}(K)\right]\hat{\beta}(K)\right\} \tag{6}$$

By introducing the Fourier transform of the indicial function, expressed by Eq.(7), into Eq.(6), the frequency domain pressure mode coordinate can be presented by Eq.(8).

$$\begin{aligned}\varphi(0)+\hat{\varphi}'(K)&=1-\sum_{k=1}^{2}a_k+\sum_{k=1}^{2}\frac{a_k d_k^2}{d_n^2+K^2}-\mathrm{i}K\sum_{k=1}^{2}\frac{a_k d_k}{d_k^2+K^2}\\&=1-K^2\sum_{k=1}^{2}\frac{a_k}{d_k^2+K^2}-\mathrm{i}K\sum_{k=1}^{2}\frac{a_k d_k}{d_k^2+K^2}\end{aligned} \tag{7}$$

$$\begin{aligned}\hat{\alpha}_j(K)=\frac{1}{2}\rho\bar{U}^2\Bigg[&2C_{\alpha_j}\left(1-K^2\sum_{k=1}^{2}\frac{a_{\alpha_j u,k}}{d_{\alpha_j u,k}^2+K^2}-\mathrm{i}K\sum_{k=1}^{2}\frac{a_{\alpha_j u,k}d_{\alpha_j u,k}}{d_{\alpha_j u,k}^2+K^2}\right)\frac{\hat{u}(K)}{\bar{U}}\\&+C'_{\alpha_j}\left(1-K^2\sum_{k=1}^{2}\frac{a_{\alpha_j w,k}}{d_{\alpha_j w,k}^2+K^2}-\mathrm{i}K\sum_{k=1}^{2}\frac{a_{\alpha_j w,k}d_{\alpha_j w,k}}{d_{\alpha_j w,k}^2+K^2}\right)\frac{\hat{w}(K)}{\bar{U}}\\&-C'_{\alpha_j}\left(1-K^2\sum_{k=1}^{2}\frac{a_{\alpha_j h,k}}{d_{\alpha_j h,k}^2+K^2}-\mathrm{i}K\sum_{k=1}^{2}\frac{a_{\alpha_j h,k}d_{\alpha_j h,k}}{d_{\alpha_j h,k}^2+K^2}\right)\mathrm{i}K\frac{\hat{h}(K)}{B}\\&+C'_{\alpha_j}\left(1-K^2\sum_{k=1}^{2}\frac{a_{\alpha_j \beta,k}}{d_{\alpha_j \beta,k}^2+K^2}-\mathrm{i}K\sum_{k=1}^{2}\frac{a_{\alpha_j \beta,k}d_{\alpha_j \beta,k}}{d_{\alpha_j \beta,k}^2+K^2}\right)\hat{\beta}(K)\Bigg]\end{aligned} \tag{8}$$

On the other hand, the aeroelastic component of each pressure mode coordinate can be expressed in a similar was to the conventional self-excited force by introducing pressure modal derivatives.

$$\hat{\alpha}_{j,se}(K)=\frac{1}{2}\rho\bar{U}^2K^2\left[\left(\mathrm{i}X^*_{\alpha_j 1}+X^*_{\alpha_j 4}\right)\hat{h}(K)/B+\left(\mathrm{i}X^*_{\alpha_j 2}+X^*_{\alpha_j 3}\right)\hat{\beta}(K)\right] \tag{9}$$

where $X^*_{\alpha_j 1}\sim X^*_{\alpha_j 4}$ are the pressure modal derivatives and can be found by comparing Eq.(9) with Eq.(8) as follows:

$$\begin{cases}X^*_{\alpha_j 1}=-C'_{\alpha_j}\left[\dfrac{1}{K}-K\displaystyle\sum_{k=1}^{2}\frac{a_{\alpha_j h,k}}{d_{\alpha_j h,k}^2+K^2}\right]\\ X^*_{\alpha_j 4}=-C'_{\alpha_j}\displaystyle\sum_{k=1}^{2}\frac{a_{\alpha_j h,k}d_{\alpha_j h,k}}{d_{\alpha_j h,k}^2+K^2}\end{cases} \tag{10}$$

$$\begin{cases}X^*_{\alpha_j 2}=-C'_{\alpha_j}\dfrac{1}{K}\displaystyle\sum_{k=1}^{2}\frac{a_{\alpha_j \beta,k}d_{\alpha_j \beta,k}}{d_{\alpha_j \beta,k}^2+K^2}\\ X^*_{\alpha_j 3}=C'_{\alpha_j}\left[\dfrac{1}{K^2}-\displaystyle\sum_{k=1}^{2}\frac{a_{\alpha_j \beta,k}}{d_{\alpha_j \beta,k}^2+K^2}\right]\end{cases} \tag{11}$$

2.3. Relationship between Pressure Mode and Force Derivatives

The lift force is taken as an example to explain the relationship between the POD pressure mode and force derivatives. The relationship among the force, pressures, and POD pressure modes can be found

$$F_L=\sum_{i=1}^{N}P_i\delta_i\sin(\varphi_i-\theta)\approx\sum_{i=1}^{N}\sum_{j=1}^{\tilde{N}}\alpha_j\phi_{ij}\delta_i\sin(\varphi_i-\theta) \tag{12}$$

Moreover, the aeroelastic component can be expressed separately

$$F_{L,se}=\sum_{i=1}^{N}P_{i,se}\delta_i\sin(\varphi_i-\theta)\approx\sum_{i=1}^{N}\sum_{j=1}^{\tilde{N}}\alpha_{j,se}\phi_{ij}\delta_i\sin(\varphi_i-\theta) \tag{13}$$

The common expression for self-excited lift force is given by

$$F_{L,se}(K)=\frac{1}{2}\rho\bar{U}^2BK^2\left[\left(\mathrm{i}H_1^*+H_4^*\right)h/B+\left(\mathrm{i}H_2^*+H_3^*\right)\beta\right] \tag{14}$$

By comparing Eq.(13) with Eq.(14), the relationship between conventional flutter derivatives and pressure model derivatives can be found as

$$\begin{cases}H_1^*=\dfrac{1}{B}\displaystyle\sum_{i=1}^{N}\sum_{j=1}^{\tilde{N}}X^*_{\alpha_j 1}\phi_{ij}\delta_i\sin(\varphi_i-\theta)\\ H_4^*=\dfrac{1}{B}\displaystyle\sum_{i=1}^{N}\sum_{j=1}^{\tilde{N}}X^*_{\alpha_j 4}\phi_{ij}\delta_i\sin(\varphi_i-\theta)\end{cases} \tag{15}$$

$$\begin{cases}H_2^*=\dfrac{1}{B}\displaystyle\sum_{i=1}^{N}\sum_{j=1}^{\tilde{N}}X^*_{\alpha_j 2}\phi_{ij}\delta_i\sin(\varphi_i-\theta)\\ H_3^*=\dfrac{1}{B}\displaystyle\sum_{i=1}^{N}\sum_{j=1}^{\tilde{N}}X^*_{\alpha_j 3}\phi_{ij}\delta_i\sin(\varphi_i-\theta)\end{cases} \tag{16}$$

3. Wind Tunnel Tests

The pressure tests on a spring-suspended sectional model were carried out in the TJ-2 Wind Tunnel in Tongji University, as shown in Figure 2. The model section represents the typical deck geometry of the Stonecutters Bridge with a length scale of 1:50. The model is 1.740m in length and 1.066m in width with a 0.286m wide slot between the two decks. 49 pressure taps were arranged around one single box. The vertical and torsional nature frequencies of the sectional model were identified to be 2.05Hz and 3.71 Hz, respectively.

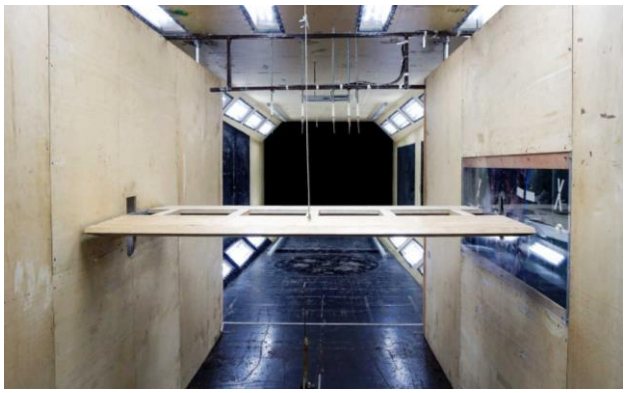

Figure 2 Wind tunnel pressure test setup

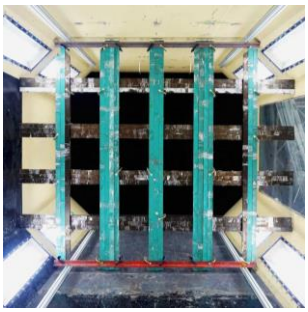

Figure 3 Turbulence simulation fence

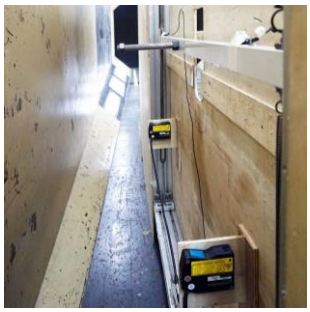

Figure 4 Springs and sensors

During the test, the turbulent wind was simulated by a fence installed at 8.5m upstream of the model (see Figure 3). The turbulent wind was recorded by the cobra probes shown in Figure 1, and the vertical and torsion motions were recorded by the laser displacement sensors shown in Figure 4.

4. Results and Discussions

4.1. POD Pressure Modes

A turbulent wind field with 0° attack angle, 10.36 m/s mean velocity, 10.60% longitudinal turbulence intensity and 8.85% vertical turbulence intensity is selected to investigate the characteristics of distributed aerodynamic and aeroelastic pressures. The POD method is employed to decompose the pressure field into a series of pressure modes. The space functions and the power spectra of the principle coordinates of the first four POD pressure modes are shown in Figure 5 and Figure 6, respectively. The energy contribution proportions of the first fourteen POD modes are listed in Table 1.

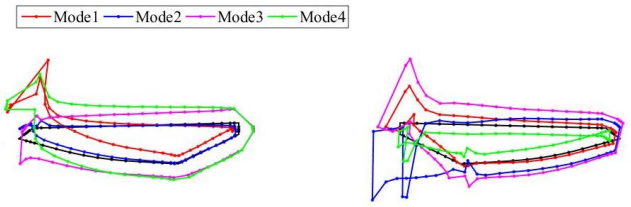

Figure 5 Space function distribution of first four POD modes

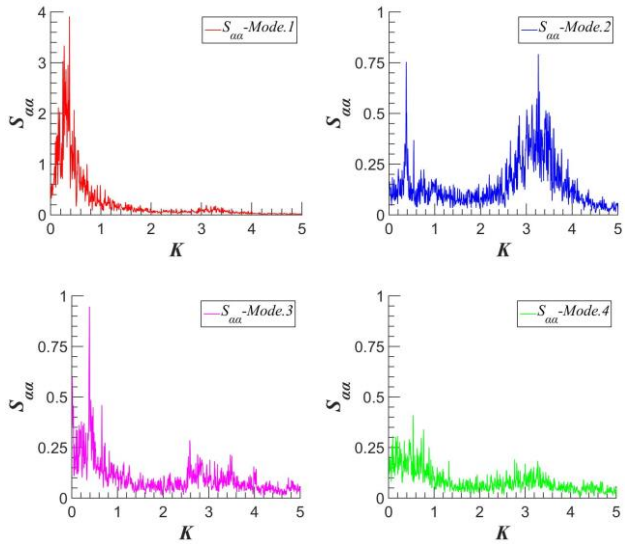

Figure 6 Principal coordinate spectra of first four POD modes

It can be seen from Figure 5 that the main variations of space functions among different POD modes concentrate on the windward edges of the two boxes, especially the downstream box. This indicates that the windward region plays more significant role in distributed fluctuating pressures. Figure 6 suggests that the first pressure mode contributes the most (using different y-axis values for a clear depiction). Additionally, the wind-induced aerodynamic component is mainly represented by the first POD mode, while the self-excited aeroelastic component is reflected by the second and the third modes. Moreover, the signature turbulence is basically reflected by the second modes. The fourth mode contributes little to the fluctuating pressures

Table 1 Energy contribution proportions of first fourteen POD modes

Mode No.	E_{ϕ_j} (%)	$\sum E_{\phi_j}$ (%)	Mode No.	E_{ϕ_j} (%)	$\sum E_{\phi_j}$ (%)
1	25.23	25.23	8	2.16	81.60
2	16.71	41.94	9	2.00	83.60
3	15.15	57.09	10	1.94	85.54
4	11.87	68.96	11	1.54	87.08
5	4.76	73.71	12	1.40	88.48
6	3.36	77.07	13	1.15	89.63
7	2.37	79.44	14	1.02	90.65

As shown in Table 1, the energy proportion falls rapidly with the increase of mode order, and the fluctuating pressures can be reconstructed using a limited number of the low-order POD modes. For example, fourteen modes have been used to reconstruct the pressure field with an energy threshold of 90%.

4.2. Pressure Modal Derivatives

Table 2 gives out the indicial function parameters of the first four POD modes identified by the least square method with Eq.(8). The pressure modal derivatives can then be calculated by Eq.(10)-(11) and shown in Figure 7. Table 2 shows that the values of a_1 are closer to 1, especially for those related to h and β, which indicates that the corresponding indicial functions are very small. On the other hand, the very small d_1 suggests a relatively slow decay, especially for the β related indicial functions. Additionally, it can be noticed from Figure 7 that the β related derivatives, especially $X^*_{\alpha_j 3}$, are much larger than the other modal derivatives. The aeroelastic components of the first and the fourth modes are mainly controlled by $X^*_{\alpha_j 3}$.

Table 2 Indicial function parameters of first four POD modes

Mode	φ	a_1	d_1	a_2	d_2
1	$\varphi_{\alpha_1 h}$	1.0084	0.0001	0.0010	0.0100
	$\varphi_{\alpha_1 \beta}$	1.0397	0.0001	0.0010	0.0100
	$\varphi_{\alpha_1 u}$	1.7762	0.0039	0.0050	0.0100
	$\varphi_{\alpha_1 w}$	1.0296	0.0217	0.0010	0.0100
2	$\varphi_{\alpha_2 h}$	1.1430	0.1279	0.0011	0.0100
	$\varphi_{\alpha_2 \beta}$	1.1473	0.0279	0.0014	0.0100
	$\varphi_{\alpha_2 u}$	0.9356	0.0597	0.0010	0.0100
	$\varphi_{\alpha_2 w}$	0.8063	0.0028	0.0284	0.2623
3	$\varphi_{\alpha_3 h}$	0.9625	0.0668	0.0670	0.0100
	$\varphi_{\alpha_3 \beta}$	1.1536	0.0001	0.0010	0.0100
	$\varphi_{\alpha_3 u}$	0.9215	0.0001	0.2528	0.4099
	$\varphi_{\alpha_3 w}$	0.6186	0.0044	0.0066	0.0100
4	$\varphi_{\alpha_4 h}$	1.0007	0.0019	0.0157	0.0100
	$\varphi_{\alpha_4 \beta}$	0.9875	0.0001	0.0010	0.0100
	$\varphi_{\alpha_4 u}$	0.9396	0.0004	0.0011	0.0100
	$\varphi_{\alpha_4 w}$	0.9975	0.0021	0.0010	0.0100

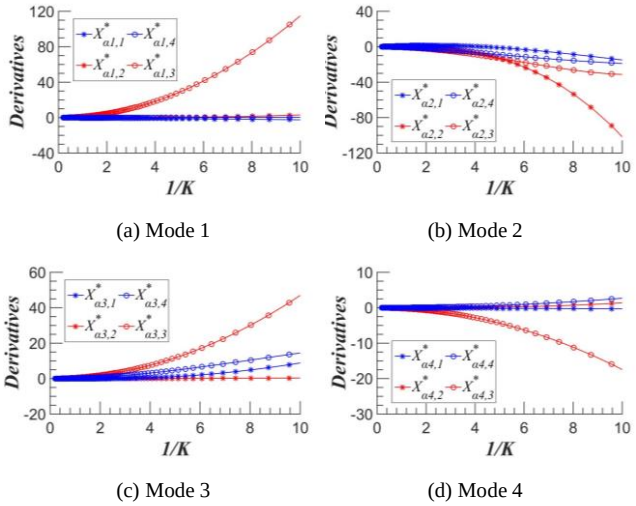

(a) Mode 1 (b) Mode 2

(c) Mode 3 (d) Mode 4

Figure 7 Pressure modal derivatives of first four POD modes

4.3. Aerodynamic and Aeroelastic Pressures

Two taps near windward edges of each box are selected as key points to exemplify the feasibility of pressure reconstruction using the POD modes (see Figure 1). The measured pressure time

histories and spectra, as well as the divided aerodynamic and aeroelastic components, are shown in Figure 8 and Figure 9, respectively. For the two key taps located at windward edges of each box, the pressure characters are of great difference. It can be found from the figures that the self-excited behaviour and the high-frequency signature turbulence have a bigger impact on the downstream box.

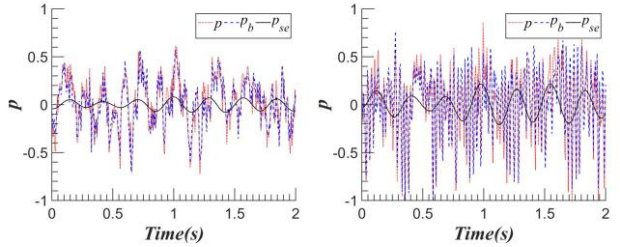

(a) Key tap 1 (b) Key tap 2

Figure 8 Aerodynamic and aeroelastic pressure time histories at key taps

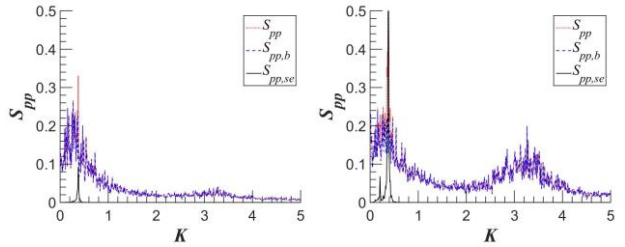

(a) Key tap 1 (b) Key tap 2

Figure 9 Aerodynamic and aeroelastic spectral components at key taps

To further investigate the influence of different POD modes, the spectral components related to the first four modes are given in Figure 10. Although the first and the second POD modes both play important roles as a whole, the proportions of different modes vary from one location to another. As the first and the second modes are mainly related to the wind-induced and the self-excited components, the first two modes are much more influential on the upstream and the downstream boxes, representatively. Moreover, the dominant mode of some pressure taps can be other POD modes rather than the first two modes.

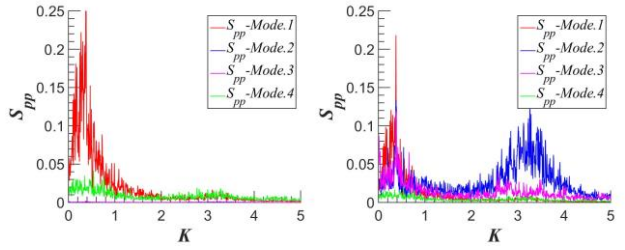

(a) Key tap 1 (b) Key tap 2

Figure 10 P Spectral components related to first four modes at key taps

4.4. Aerodynamic and Aeroelastic Forces

The aeroelastic force admittances can be obtained using Eq.(15)-(16), while the reconstructed aeroelastic derivatives of lift and moment are plotted in Figure 11. The aerodynamic and aeroelastic spectra of integral forces can also be calculated with the already recognized aerodynamic and aeroelastic pressures and plotted in Figure 12. It can be observed from Figure 11 and Figure 12 that the lift force is significantly larger than the moment, and thus the lift related derivatives are much bigger than moment related ones. Moreover, the moment related components are confirmed to be more crucial than lift related ones.

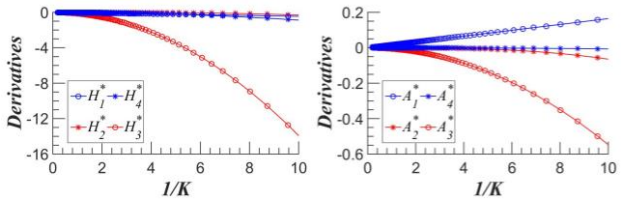

(a) Lift force (b) Pitching moment

Figure 11 Reconstructed lift and moment derivatives

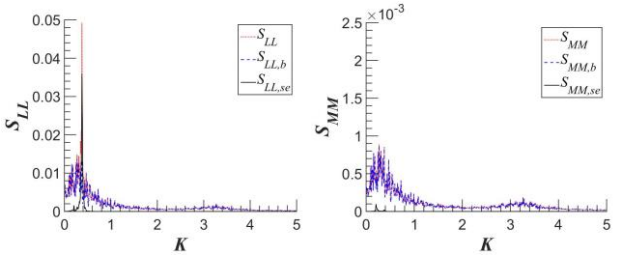

(a) Lift force (b) Pitching moment

Figure 12 Reconstructed lift and moment spectra

5. Conclusions

A proper orthogonal decomposition (POD) based modelling scheme for distributed aerodynamic and aeroelastic pressures on bridge decks has been proposed. The POD method can directly and effectively separate the principal components of fluctuating pressure and reveal the distribution characteristics. In this case study, the aerodynamic component is mainly represented by the first POD mode and dominates the upstream box, while the aeroelastic component is reflected by the second and the third modes which have a greater influence on the downstream box. Meanwhile, the distributed pressures and the integral forces can be successfully reconstructed with the POD modes. Nevertheless, further analysis should be carried out to verify the physical interpretation of the POD modes and also check the universality.

Acknowledgments

This work was supported by Hong Kong Research Grants Council [General Research Fund: PolyU15221815]; and National Natural Science Foundation of China [Grants: 51478360].

References

[1] Grenet, E.T.D. & Ricciardelli, F., Spectral Proper Transformation of Wind Pressure Fluctuations: Application to a Square Cylinder and a Bridge Deck, *J. Wind Eng. Ind. Aerodyn.*, 92, 2004, 1281-1297.

[2] Tan. Z.X., Zhu. L.D., et al., A Concept and Identification of Pressure Modal Admittance for Distributed Fluctuating Pressures on Bridge Decks, in: *Proc. 8th Int. Colloq. Bluff Body Aerodyn. Appl.*, Boston, Massachusetts, USA, 2016.

[3] Wu, T. & Kareem, A., Bridge Aerodynamics and Aeroelasticity: A Comparison of Modeling Schemes, *J. Fluids Struct.*, 43, 2013, 347-370.

[4] Scanlan, R.H., Problematics in Formulation of Wind‐Force Models for Bridge Decks, *J. Eng. Mech.*, 119(7), 1993, 1353-1375.

[5] Costa, C., Aerodynamic Admittance Functions and Buffeting Forces for Bridges via Indicial Functions, *J. Fluids Struct.*, 23, 2007, 413-428.